Generation of terahertz electric oscillations by ballistic quantized holes with negative effective mass.

Z. S. Gribnikov, A. N. Korshak, V. V. Mitin
Department of Electrical and Computer Engineering,
Wayne State University, Detroit, MI, 48202

The dispersion relation for the ground subband of quantized holes in a quantum well (QW) of zink-blende-like semiconductors contains an extensive section with negative effective mass (NEM). Under certain biases, stationary concentration distributions of the ballistic quantized holes in p^+pp^+-structures hold a self-organized region where holes with NEM predominate. The existence of such region causes a global instability of the entire stationary regime and the appearance of an oscillatory regime. We describe the dependence of the oscillatory regime on material and geometric parameters of the structure and consider factors that influence the oscillation frequency. The typical frequencies for 0.1 μm-structures are in the terahertz range (1-2 THz). The ballistic NEM-diodes have been classified as short, medium and long diodes depending on their oscillatory portrait. A new high-voltage region of oscillations that was not analytically predicted in early works is revealed in the so-called medium and long diodes. The region appears side by side with the stable stationary regime at high voltages. Switching between oscillatory and stationary regimes is studied.

We also discuss the feasibility of ballistic transport of quantized holes in GaAs/AlAs p-QWs and substantiate a method of computer plotter of characteristics for a description of nonstationary processes.

I. Introduction

As was shown in previous works of our group [1,2,3], a section with negative effective mass (NEM) in a dispersion relation of current carriers causes instability of stationary ballistic current in short p^+pp^+-diodes. This instability is due to self-organized quasineutral plasma region with predominating NEM-carriers at certain voltages across the diode. A homogeneous NEM-plasma is convectively unstable for arbitrary wave vectors of fluctuations and increment of this instability is numerically equal to the plasma frequency determined by the NEM:

$$\eta = \sqrt{\frac{e^2 N}{\kappa_d m_N}}, \qquad (1)$$

where N is a doping concentration (equal to the concentration of the NEM-carriers in the NEM-plasma), κ_d is a dielectric constant, $m_N = |\partial^2\varepsilon/\partial p_x^{\,2}|^{-1}$ is a value of the NEM, ε is an energy, and $\boldsymbol{p}$ is a momentum. This convective instability in diodes that are short-circuited or loaded with a small resistance is globalized and results in current oscillations accompanied by oscillations of carrier concentration and electric field[3-5].

The oscillations appear in a particular range of voltages across the diode that is determined mainly by the specific form of the dispersion relation. The oscillation frequency is higher for a shorter diode base. It is in terahertz range for submicron base lengths. Generally, the oscillation frequency increases with voltage. The current oscillations can be quasilinear (characterized basically by only one frequency) or substantially nonlinear [5,6] (characterized by a number of frequencies). The latter occurs in comparatively long bases when criteria of the oscillatory regime are met with sufficient reserves.

We have considered the following media with immanent NEM-sections in the carrier dispersion relations: (i) asymmetrical double quantum wells (QWs), single and multiple, with NEM-sections due to tunnel anticrossing of two initial dispersion relations of the formative QWs [3,4,6-8]; (ii) ΓX–composite QWs with ΓX–anticrossing at the sharp boundary between the Γ– and X-regions [6,8,9]; (iii) uniaxially compressed (or tensile-stressed in the plane) p-type cubic semiconductors with degenerate (before deformation) valence band [10-12]; and (iv) p-type QWs, single or multiple, in cubic semiconductors. This last mechanism is the subject of our consideration here.

Also, we turn our attention to the NEM-sections in the calculated electron and hole dispersion relations for bulk semiconductors. These sections are in dispersion relations of Γ–electrons in cubic semiconductors along the <111>-axes on the way to the saddle points from Γ–valleys to L-valleys [13,14]. The effective mass of Γ–electrons becomes negative beginning from energies ε_1~0.5 eV. These energies can be lower than the energies of bottoms of L- and X-valleys. This is very important for holding a ballistic transport. The characteristic energies for this mechanism are much greater than analogous energies for all the above-mentioned mechanisms. Therefore, much shorter base lengths and much higher oscillation frequencies are expected for this case. The NEM-sections are in hole dispersion relations in wurzites along the directions perpendicular to the hexagonal axis (see Ref. 15 as a review).

The NEM-section in the ground subband HH1 of the dispersion relation for quantized holes (Fig. 1(a)) appears due to the spin-orbit coupling of heavy- and light-hole states at the sharp sidewalls of a QW. Besides, the longitudinal effective mass in the bottom of the subband is small. It is substantially smaller than heavy hole mass and slightly greater than the light hole mass [16-19]. The substantial reduction in the effective mass of the HH1-holes for small $\boldsymbol{p}$ must

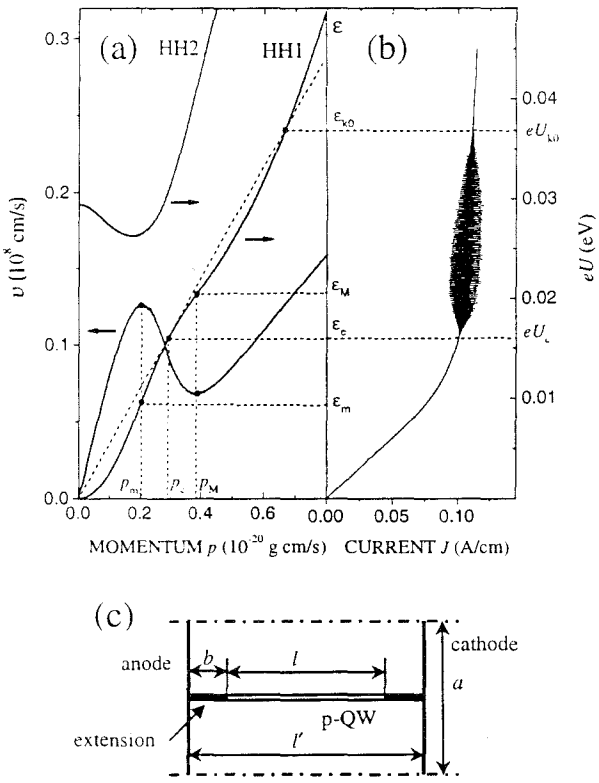

Figure 1. (a) The two lowest subbands (HH1 and HH2) of hole dispersion relation, $\varepsilon(p)$, and velocity, $v(p)$, of HH1-holes in GaAs/AlAs p-QW of 80 Å width. (b) The IV-characteristic, $J(U)$, with an oscillatory regime for the basic sample (1.1). To show a relation of the oscillatory regime with parameters of the dispersion relation, $J(U)$-curve is plotted with the vertical U-axis that is linked to the ε-axis of $\varepsilon(p)$ plot. (c) Geometry of the model element of the spatial periodic structure.

increase their mobility and mean free path. This is especially important to keep transport in the QW ballistic.

NEM-sections also appear in all the exited subbands of the hole spectrum. But exploitation of these sections is difficult because we can not separate holes from different subbands with different effective masses that carry current through the base. As a result, unmixed carrier plasma with only the NEM-holes can not be formed. An analogous problem occurs in substantially asymmetrical quantum well that appears at a modulation-doped heterojunction (MDH QW) [20]. In this case, lifting of the twofold spin degeneracy splits the subband HH1 in two: $HH1^{(\pm)}$. Therefore, for the ballistic diode base, we need a narrow symmetrical square p-type QW with sharp and plane confining sidewalls. There are abundant proofs of very high hole mobility in MDH QWs and in wide square QWs (of 11-15 nm width) grown on <311>A-GaAs-

substrates. But we have no such a reliable evidence for narrower QWs. Since the feasibility of the hole ballistic transport in p-QWs for reasonable base lengths (0.05-0.5 μm) is very important for our consideration, we discuss this problem in detail in Appendix. Below, we consider GaAs/$Al_xGa_{1-x}As$ p-QWs with high Al content (usually x=1) in the barriers. At the present time, only these QWs can exhibit the high mobilities and long ballistic mean free paths, which are required for terahertz generation. Some preliminary results on the ballistic quantized hole transport and terahertz generation in p^+pp^+-diodes were reported at several conferences and were published in their proceedings [21-24].

In the following sections, we present a list of basic equations and assumptions substantiating a computer plotter of current-voltage (IV) characteristics (CP IVC) – the main computing method used in this work (Sec. II); detail dependence of an oscillatory regime on material and geometric parameters of the structure and present the characteristic values of oscillation frequencies for the selected design and material systems (Secs.III and IV); describe and explain an inner picture of the oscillatory regime that is temporary-spatial organization of hole concentration distributions (Sec. V); and discuss at length a new high voltage oscillatory regime and briefly consider opportunities of rising frequency limits (Sec. VI).

II. Basic Equations and Assumptions: Computer Plotter of Characteristics

We consider the two-dimensional (2D) Poisson problem in a rectangle of length $l'=l+2b$ along the x-axis and width a along the y-axis with boundary conditions of periodicity at $y=\pm a/2$ planes. Each spatial period includes one p-QW (see Fig. 1(c)) with ballistic transport of quantized holes in it. The dispersion relation of these holes is calculated preliminarily in the two-band approximation (4×4 Hamiltonian) for a symmetric square QW with the given Lattinger parameters [10] in the well and in the barriers. The two lowest subbands of the quantized holes are shown in Fig. 1(a). Usually, calculations of the quantized holes spectra are not restricted to the two-band approximation and take into account the spin-split valence band (6×6 Hamiltonian) and even the distant conductivity band[25,26] (8×8 Hamiltonian). These calculations demonstrate that the two-band approximation is of sufficient preciseness for the ground subband, which is of our interest here. The obtained dispersion relation is taken unchanged for all currents and voltages despite different hole population and transverse electric fields.

We consider nonstationary classical (Newton) transport of holes within the ground HH1-subband only. The p^+-contacts do not emit holes either into the higher subbands or into the barriers. The ballistic kinetic equation for one-dimensional hole transport along the x-axis in the p-QW and the 2D-Poisson equation in the p-QW and in the barriers are solved selfconsistently for a given

distribution of acceptors in the barriers (the modulation doping). A system of boundary conditions is as follows. 1). Potentials of the anode, $V_a=0$, and the cathode, $V_c=U$, are given (excluding a regime with an outer load; detailed results for this regime will be collected elsewhere). 2). Distribution functions of the holes entering the base from the anode, $f_a^{(+)}(\boldsymbol{p})$, and the cathode, $f_c^{(-)}(\boldsymbol{p})$, are selected in the form of Fermi-functions with the Fermi-energies $\varepsilon_F^{(a,c)}$. These Fermi-energies are equal to each other and exceed the equilibrium Fermi-energy of quantized holes in the base determined by the doping per QW. Due to weakness of 2D-screening, the accumulation regions near the anode and cathode penetrate deeply into the base. 3). No reflection of the holes reached the cathode and the anode is suggested. Neither kinetic nor electrostatic problems are solved within the p^+-contacts. The contacts are determined completely by the above-formulated boundary conditions.

The shape of the p^+-electrodes affects the solution of the Poisson problem in the base. The diode shown in Fig. 1(c) is similar to a flat capacitor with plates positioned at distance $l+2b$, where l is the length of p-QW-channel (the base length) and b is the length of the electrode extensions. These extensions are flat contacts to the p-QW of the same width w. Three sizes a, b, l allow us to vary a spatial problem. The condition $a>l$ corresponds to almost a single (solitary) QW, $b>>a$ is a case of flat 2D-contacts while $b=0$ is a case of massive 3D-contacts to the QW.

The scheme of the numerical solution of the nonstationary 2D-problem has been described in great detail in Ref. 6. The QW in the y-axis direction is presented always as a single cell. This means that we neglect transverse electric fields in it. We obtain nonstationary 1D-distributions of hole concentration and electric potential along the QW ($0<x<l$) and 2D- distributions of the potential in the whole diode and then calculate the 1D-hole current in the QW, $j_p= j_{px}(x,t)$, and 2D-displacement current everywhere. Finally, we calculate the total current per one spatial period of the structure, $J(t)$, and plot an IV-characteristic using a CP IVC described in our previous works [4-6,12].

We apply a time-dependent voltage $U(t)$ across the diode, which is usually chosen as a linear function of a time:

$$U(t) = U(0) + U' \times t \,. \qquad (2)$$

The voltage sweep rate $|U'|$ is taken to be small enough to keep the process adiabatic. Calculated $J(t)$-dependency describes an IV-characteristic of the diode if it is static and portrays the current oscillations in the generation regime (see Fig. 1(b)). Naturally, the voltage sweep rate should be slow enough to accommodate a large number of periods of the current oscillations in the interval from U_c to U_{k0}:

$$\langle f \rangle \frac{U_{k0} - U_c}{|U'|} >> 1, \qquad (3)$$

where $\langle f \rangle$ is a mean value of an oscillation frequency $f=\omega/2\pi$. This necessary condition can be insufficient in cases of very slow relaxation of exited oscillations or delayed arising of the oscillatory regime. A characteristic relaxation time, t_r, can be much greater than the oscillation period, $T=f^{-1}$, for example, we have fixed $ft_r \sim 20$. The existence of such slow processes imposes additional condition on $|U'|$:

$$U_{k0} - U_c >> t_r |U'|. \qquad (4)$$

High sweep rate leads to a false increase in U_k (see Fig. 2(a)). More serious requirements for U' come from multivalued behavior of the IV-characteristics. We have revealed a hysteresis near U_c and U_k. There are two values of voltage U_c (further U_c and U_c', $U_c'>U_c$) and two values of voltage U_k (further U_k and U_k') showed in Fig. 2 (b). For $U'>0$ (a forward direction), oscillations start (U_c') and finish (U_k) at higher voltages than they finish (U_c) and start (U_k') for $U'<0$ (a reverse direction). This means that in the intervals (U_c, U_c') and (U_k', U_k) there are stationary nonoscillatory "overheated" and "overcooled" states side by side with the oscillatory regimes. Often, these intervals are not small. While measuring U_c' (for the forward direction) and U_k' (for the reverse direction), U' has to be chosen very small because an increased rate shifts U_c'

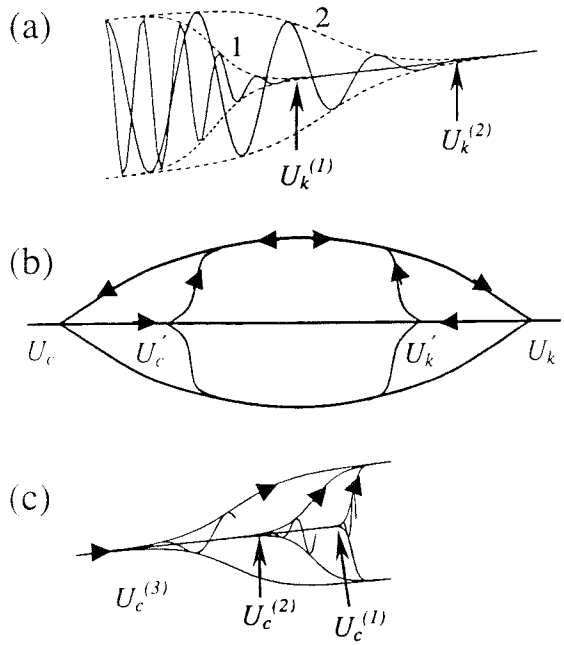

Figure 2. (a) Dependence of voltage U_k on voltage sweep rate U': $U'^{(2)} > U'^{(1)}$. (b) Schematic of an oscillatory portrait for forward and reverse direction of the CP IVC. (c) Dependence of voltage U_c' on voltage sweep rate U': $U'^{(3)} > U'^{(2)} > U'^{(1)}$.

to U_c and U_k' to U_k. The overheated and overcooled states are weakly metastable near the points U_c' and U_k'; they are destroyed by even very small embryonic fluctuations. Since the voltage variation in the computer version is a discrete process, a faster voltage sweep rate causes greater voltage fluctuations. As a result, the critical points $U_c^{(1,2,3)}$ (see Fig. 2(c)) of the nonstationary regime shift further from the real critical point U_c'. Evidently, abrupt (shock) changes of the voltage can destroy the metastable regimes and display an incomplete picture of oscillations. On the other hand, oscillatory regimes that are not accessible for adiabatically slow voltage changes exist: these oscillations can be turned on by a voltage shock only.

In summary, we note the following. 1). The voltage sweep rate U' has to be sufficiently small to keep the process adiabatic. It is extremely important near the points U_c, U_k, U_c', and U_k'. 2). Passing the entire oscillation region in forward and reverse directions could reveal both overheated and overcooled regions. 3). When no oscillations appear in an adiabatic process, turning a shock voltage on could reveal the oscillatory regime.

III. Current Oscillations

The existence of the oscillatory regime and its features depend on four groups of parameters of the ballistic diode structure and on operations conditions. In the first place, this is the voltage across the diode U. Dependence on U can be multivalued. In the second place, these are parameters of the dispersion relation - an energy position of the NEM-section and dependence of hole velocity on momentum, which are determined by the Luttinger parameters for well and barriers, and the QW width, w. In the third place, these are three geometric parameters l, a, b (Fig. 1(c)). And in the fourth place, these are concentration parameters - acceptor concentration per one QW, N_A, and the Fermi-energy, $\varepsilon_F^{(c)}$, of holes entering the base from the p^+-contacts. We have to add a temperature T and dielectric constants for the QW (κ_{dW}) and the barriers (κ_{dB}) to this list. In addition, there are a number of implicit parameters such as optical phonon energy and mean scattering time. For example, since transport in the base is supposed to be ballistic, hole energies must not exceed the optical phonon energy $\hbar\omega_0$. This energy restricts our choice of p-QW parameters. In particular, the characteristic energy of NEM- holes, ε_c, has to be smaller than $\hbar\omega_0$ to have a sufficiently wide voltage interval (ε_c/e, $\hbar\omega_0/e$) for the oscillatory regime. The selected value ε_c determines the upper limits of doping concentration N_A and the Fermi-energy $\varepsilon_F^{(c)}$. All together conduce to the minimum base length allowing the oscillatory regime and, therefore, to the maximum attainable frequency of oscillations. The mean free path due to roughness and residual impurity scattering (implicit parameters) limits the maximum base length.

Below, we present results obtained with the dispersion relation shown in Fig. 1(a). This dispersion is related to GaAs/AlAs-QW with w=8 nm and the Luttinger parameters: γ_1=6.9, γ_2=γ_3=2.5 in GaAs and γ_1=4.0, γ_2=γ_3=1.3 in AlAs. Corresponding energy $\varepsilon_c \approx 17$ meV is much smaller than $\hbar\omega_0$=36 meV for GaAs. The other parameters are: T=4.2 K and $\kappa_{dW}=\kappa_{dB}$=10.9. As a basic sample we select the diode with b=0, $l'=l_0$=0.1 μm, $N_A=N_0=6\cdot10^{10}$ cm^{-2}, $\varepsilon_F^{(c)}$=10 meV, and $a=a_0$=32 nm. Current –voltage characteristic for this sample calculated by the CP IVC is shown in Fig. 1(b), and also in Figs. 3(a) and (b) (curve (1.1)), 4 (curve for 0.1 μm), and 5 (curve for 10 meV). It contains an oscillation interval with $U_c \approx 17$ meV, $U_c' \approx 22.5$ meV, $U_k' \approx 28$ meV, and, $U_k \approx U_{k0} \approx 36$ meV.

Figure 3(a) shows three sets of IV-characteristics for samples with b=0, l=0.1 μm, $\varepsilon_F^{(c)}$=10 meV, N_A=X·N_0, and a=Y·a_0. They are designated as (X,Y). An increase or decrease in the spatial period (samples (1,3/2) and (1,1/2) result in different and drastic changes compared to the basic sample (1,1). There are no oscillations in sample (1,3/2) at all, whereas in sample (1,1/2) the oscillation interval is two and half times wider than in sample (1,1), and the oscillation amplitude is much greater. This extension is due to a new high-voltage region of oscillations outside the ordinary interval (ε_c/e, ε_{k0}/e), where the energies ε_c and ε_{k0} are determined by the point of tangency and the point of intersection of the $\varepsilon(p)$-curve by a straight line emerging from the origin of coordinates in Fig. 1(a). According to Refs.1, 2 these points correspond to two quasineutral regions in the base: the NEM-plasma region in the middle (ε_c), and the cathode-adjacent region with a mixed plasma where the oscillations are damped (ε_{k0}). Oscillations outside this voltage interval represent a new oscillatory regime that was not predicted in early papers. In our transferring from sample (1,1) to samples (1,1/2) and (1,3/2), we have not changed the doping concentration per one QW. This means that the obtained effects are due to a change in 2D-screening. The screening weakens with increasing a, that is with gradual 3D-2D-screening transition.

The set of samples (1/2,1/2), (1,1), and (2,2) with a constant "bulk" concentration N_A/a demonstrates almost the same drastic effects but of the opposite sign. Oscillatory activity increases and the oscillation interval expands to higher voltages with increasing a. These results confirm the important role of the correlation between a certain effective length of screening and the base length l. Another confirmation is presented in the other set of samples in Fig. 4: (5/3,1), (4/3,1), (1,1), (5/6,1), and (2/3,1), with different doping concentrations (N_A=10, 8, 6, 5, and $4\cdot10^{10}$ cm^{-2}, respectively). We see a quick decrease in amplitude and in the interval of oscillations with decrease in N_A (dawn to zero for $N_A=4\cdot10^{10}$ cm^{-2} and a=32 nm). Figure 4(a) displays an analogous degradation of the oscillatory regime when the base length l is shortened.

In comparison with the tendencies observed in Figs. 3 and 4, dependence of the oscillatory regime on the Fermi-energy $\varepsilon_F^{(c)}$ shown in Fig. 5

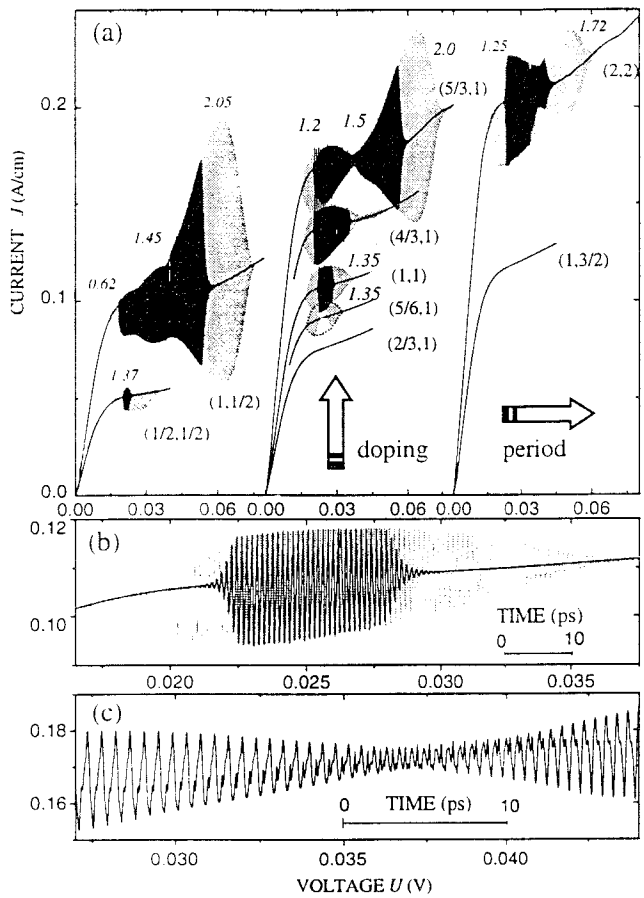

Figure 3. (a) The IV-characteristics, $J(U)$, for samples (X,Y) that differ in base doping N_A and spatial period a: N_A=X·6·10^{10} cm^{-2}, a=Y·32 nm. Curves with different Y are shifted to new origins. Directions of growth of the parameters X and Y (doping and period) are shown by arrows. Digits under the curves display frequencies of oscillations at corresponding voltages. Gray areas on the oscillatory portraits are regions that do not reproduced for forward and reverse direction of the CP IVC: voltage intervals (U_c,U_c') and (U_k',U_k) if $U_c'<U_k'$, or (U_c,U_k') and (U_c',U_k) if $U_c'>U_k'$ (see sample (5/6,1)). A black area is a reproduced region: voltage interval (U_c',U_k'). It does not exist if $U_c'>U_k'$. (b) The oscillatory portrait for sample (1,1). (c) A detail of the oscillatory portrait of sample (5/3,1): the neck between the LVR and HVR.

seems more complicated. A comparison of oscillatory portraits for sample (1,1) with different $\varepsilon_F^{(c)}$ demonstrates the existence of a certain optimal value, 6-10 meV, for which the amplitude of oscillations and their interval are developed maximally. Analogous effects have already described in Refs. 22, 23 for other

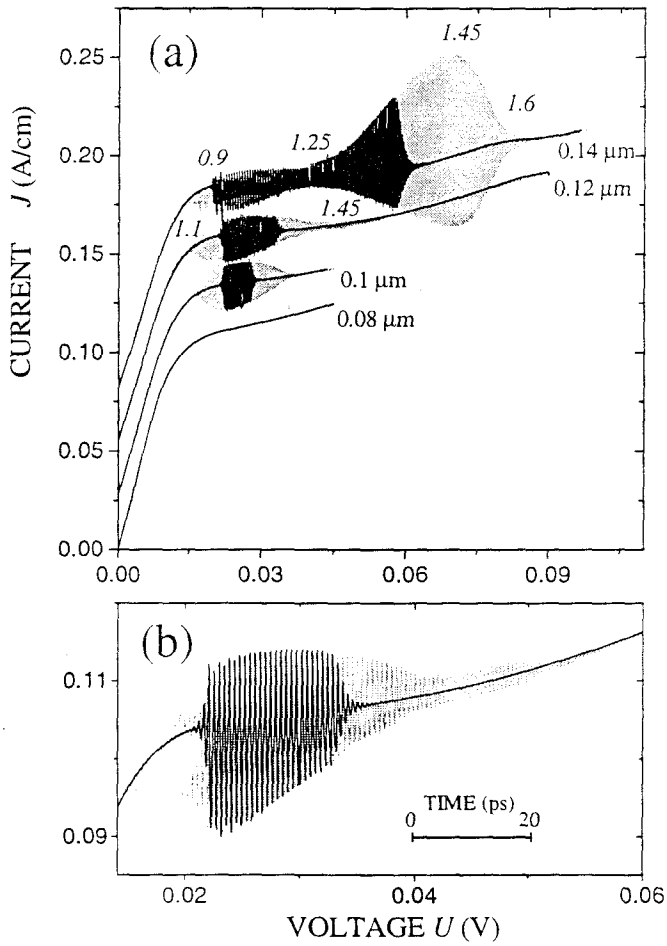

Figure 4. (a) Dependence of the oscillatory regime on the base length: a set of the IV-characteristics for diodes with different l. Base length is shown near the curves. The convention on digits and colors is the same as in Fig. 3(a). (b) The oscillatory portrait for 0.12 μm-base diode.

sets of samples. Enlarging of $\varepsilon_F^{(c)}$ increases the initial (equilibrium) hole concentration in a sample and, as a result, decreases the screening length. Nevertheless, the oscillatory activity does not strengthen and tends down if $\varepsilon_F^{(c)}$ exceeds the optimal value. This is because of the increase in concentration of background equilibrium holes with positive effective mass while concentration of the NEM-holes remains almost the same. Plasma with an increased content of holes with positive effective mass is more stable. Therefore, the oscillatory regime is degraded.

The previous results are related to the simplest contact system with b=0. "Quasimetallic" extensions of length b change an electric field distribution

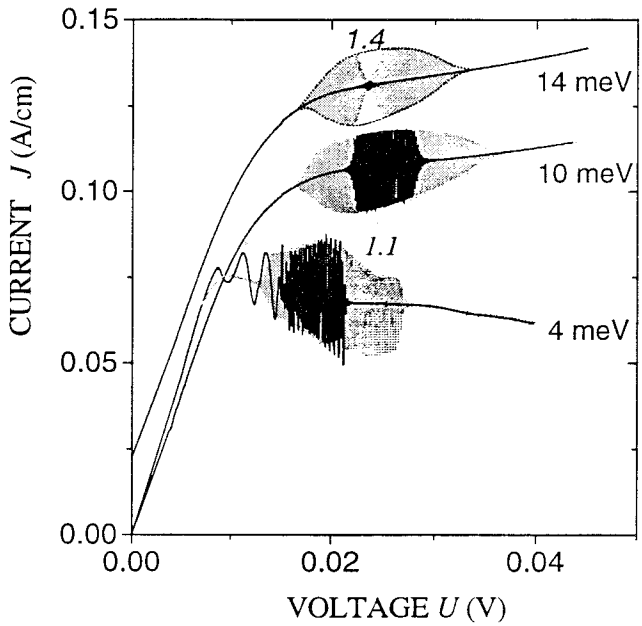

Figure 5. A set of the IV-characteristics for diodes with different Fermi-energies $\varepsilon_F^{(c)}$. The convention on digits and colors is the same as in Fig. 3(a).

in the diode base and, especially, near the edges of these extensions. A picture of 2D-screening is changed. An increase in the length b strengthens the oscillatory activity of samples other things being equal. A set of oscillatory portraits for samples with different b is presented in Fig. 6. These portraits are obtained for the comparatively long bases: l=0.2 μm. Therefore, they contain some nonlinear fragments. We see that even the very short extensions, being concentrators of the electrical field near the anode and the cathode, strengthen the oscillatory activity noticeably. They increase the voltage interval of oscillations (especially a high-voltage part) and change an oscillatory regime in a low-voltage part.

Besides the above-mentioned influence of the extensions on the detailed structure of an electrical potential near the p^+-contacts (in particular in the part of the effective anode), they also decrease channel-to-contacts capacity that shunts the diode in the oscillatory regime. This results in enhancement of the oscillatory activity in the diode base.

IV. Frequency of Oscillations

The current oscillations manifest eigentones of hole concentration and electric field in nonequilibrium ballistic plasma. Neither outer cavity nor contour determines the frequency of these oscillations. Rather, it depends only

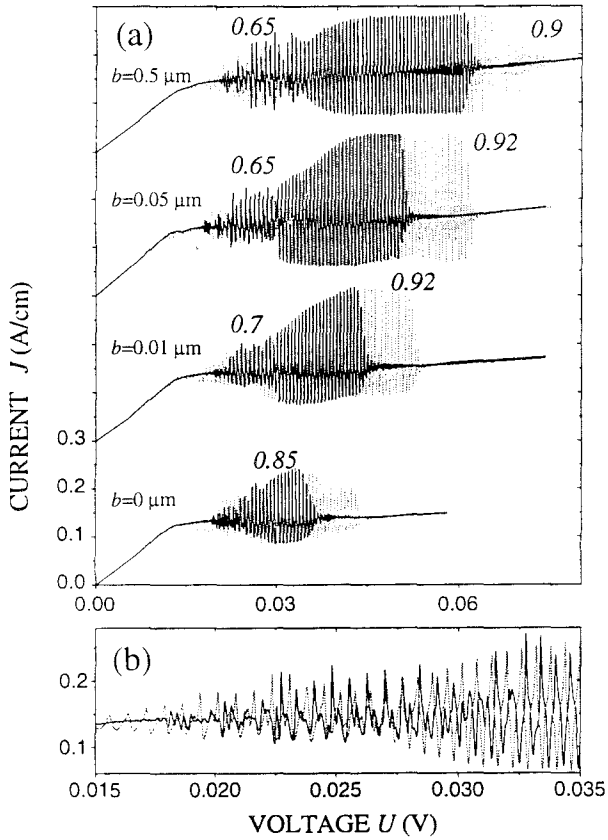

Figure 6. (a) A set of the IV-characteristics for diodes with different length of the extensions b: l=0.2 μm, a=0.4 μm, N_A=1·10^{11} cm^{-2}, $\varepsilon_F^{(c)}$=10 meV. The convention on digits and colors is the same as in Fig. 3(a). (b) A detail of the oscillatory portrait of the diode with b=0.05 μm: the picture of nonlinear oscillations.

on the inner parameters of the diode and on applied voltage U. The oscillatory regime is quasiharmonic (quasilinear) when only the fundamental harmonic predominates. It becomes more complicated and nonlinear when many harmonics is presented. The quasilinear regime is typical for short samples, when the oscillatory regime is close to critical. The nonlinear oscillations are more typical for comparatively long and heavily doped samples with well-developed oscillatory activity. Generally speaking, the frequency of oscillations increases with shortening the base and with increasing the voltage across it. But these general rules have numerous exceptions.

The oscillatory portrait of sample (1,1) in Fig. 3(b) represents the typical quasilinear regime. The nonlinear oscillations are graphically displayed for 0.2 μm-sample in Fig. 6(b). The other samples from Figs. 3-5 have sections

with nonlineary oscillations in their oscillatory portraits. In their spectral composition, the nonlinear regimes contain much higher frequencies than the fundamental frequency and these high harmonics can predominate sometimes in noticeable voltage intervals. The oscillatory portraits in which two different oscillatory regions, a low-voltage region (LVR) and a high-voltage region (HVR), are connected through a neck attract special interest. This neck shown in detail in Fig. 3(c) is a narrow interval of nonlineary oscillations with lowered amplitude. As a rule the oscillation frequency in the HVR exceeds the frequency in the LVR 1.3-1.7 times. Usually, the frequency in the HVR is highest for samples with a given base length l. On the other hand, in some samples with nonlinear oscillatory portraits there is a short-interval oscillatory regime with heightened frequency near $U=U_c$, i.e. at the low-voltage boundary of the oscillatory interval. This regime is especially interesting because it appears at low voltages: $U<\hbar\omega_o/e$.

As we have mentioned above, the voltage U controls the oscillation frequency. In Figs. 3-6, the oscillation frequencies are shown in different points of the oscillatory portraits. Sometimes, these frequencies vary slightly for samples with simple quasilinear portraits (e.g., in sample (1,1)). In such cases we indicate the single mean frequency. In the other cases, these variations are not negligible. A detailed analysis of time-dependent concentration distributions corresponding to the HVR-oscillations is given in the next section. Table 1 presents oscillation frequencies (typical numbers for the quasilinear regime and maximum numbers for the HVR) obtained for samples with different base lengths.

Table 1. Typical oscillation frequencies, f, in the LVR (below the voltage of the optical phonon emission), and maximal oscillation frequencies, f_M, for samples with different base length: [a] fundamental harmonic; [b] in the HVR; [c] in the HVR with the predominating LVR; [d] in the LVR.

l(μm)	f(THz)	f_M(THz)
0.5	0.25-0.35 [a]	0.7 [b]
0.2	0.65-0.85 [a]	1.3 [b]
0.14	0.9-1.1 [a]	1.6 [b]
0.12	1.1-1.25	1.45 [c]
0.1	1.2-1.4	2.1 [b]
0.08	2.0	2.0 [d]
0.06	2.4	2.4 [d]

To reach higher frequencies, the hole spectra should be optimized to some degree. We have to increase the energy ε_c to be just a little lower than the optical phonon energy $\hbar\omega_o$. This allows us to obtain oscillations in the shortest diode base of 0.055 μm with a maximum oscillation frequency of about 2.5 THz. Narrowing the GaAs/AlAs QW leads to heightening of the NEM-section

up to almost 0.1 eV (when ε_c and ε_k merge). As a result, we can raise the doping concentration and shorten the base length transferring the oscillation frequencies in a range 5-10 THz. This regime is realistic if ballistic hole transport could be held in the base of 25-30 nm length at voltages U~0.1-0.25 V. This is problematic even for liquid helium temperatures.

V. Spatial-Temporary Oscillations of Hole Concentration

In this section, we consider space charge waves that accompany the current oscillations in three types of diodes: (A) short; (B) medium; and (C) long.

A. Short diodes

A distinctive characteristic of the short diode is a homogeneous oscillatory region. The amplitude of the oscillations increases monotonically from zero at $U=U_c$ to a maximum value and then decreases monotonically to zero at $U=U_k$. The oscillations have quasiharmonic character and their frequency rises monotonically with voltage by no greater than 15 %. The short diodes are represented by samples (1,1) with $\varepsilon_F^{(c)}$=10 and 14 meV, (1/2,1/2), and (5/6,1) in Fig. 3 and 5.

An ordinary depletion region that develops near the anode (the left depletion region – LDR) occupies a substantial part (half or even more) of the diode base at $U\approx U_c$. If a stationary concentration distribution at $U>U_c$ were stable, it would contain a cathode-adjacent dipole layer with an accumulation layer (peak) and a depletion region (the right depletion region – RDR). Consequently, the stationary distribution consists of two depletion regions (the LDR and RDR) with the accumulation peak (AP) between them that shifts from the right to the left with increasing U over U_c. In reality, this stationary picture does not exist. Instead, a dipole wave appears in the middle of the base and grows to its termination on the cathode (Fig. 7(a)). Only one moving AP usually exists. Concentration distributions, which are similar to stationary, remain only in the left part of the diode. When an AP goes away into the cathode, it initiates the generation of a new AP in the middle of the base. This picture recalls the well-known Gunn domains (which occur for dissipative, nonballistic, carrier transport). But there is a noticeable difference. The AP in our case is formed in the middle of the homogeneous base rather than on the anode. The Gunn domains travel between the electrodes or between evidently or specially created inhomogeneities (junctions, narrowings etc). After damping the oscillations, a new stationary picture with the AP on the left and the RDR occupying most of the base is formed. The AP is separated from the anode-adjacent accumulation layer by a very narrow region with relative depletion – an LDR. This LDR narrows and the RDR widens as U increases.

B. Medium diodes

A distinctive characteristic of the medium diode is a neck in the oscillatory portrait. Such an oscillation portrait consists of two elementary

intervals, the LVR and HVR, with the neck between them (see samples (2,2), (5/3,1), (4/3,1), (1,1/2) in Fig. 3(a) and curves for l=0.12 and 0.14 μm in Fig. 4(a)). The oscillations in the medium diodes are quasiharmonic almost everywhere and they can be characterized by a fundamental frequency which is a function of voltage. A nonlinearity of the oscillations is noticeable in the neck and disappears with deepening to the LVR or to the HVR. As a rule, the neck voltage U_s (where oscillation amplitude is minimal) is near the voltage U_{k0} (Fig. 1). This means that the HVR (U_s,U_k) is usually located in the voltage region where a nonoscillatory stationary solution exists [1,2]. Existence of oscillations here represents a multivalued behavior

There are two types of oscillatory portraits for the medium diodes: (i) with a prevailing LVR (sample (4/3,1) in Fig. 3(a) and sample with l=0.12 μm in Fig. 4(a) shown in detail in Fig. 4(b)), and (ii) with a prevailing HVR (samples (1,1/2) and (5/3,1) in Fig. 3(a) and sample with l=0.14 μm in Fig. 4(a)). The HVR is not reproduced adiabatically for the reverse direction of the CP IVC. It does not appear at all for the first case and only a part of it appears for the second case.

The most important feature of the medium diode is the tuning of an oscillation frequency with voltage U. The frequency rises with voltage in each of the voltage intervals: slowly in the LVR, quicker in the HVR, and very quickly in the neck. As a result, the oscillation frequency in the medium diodes is varied in a wide range (up to 50-70 %).

There are five ways to transform a short diode into a medium one: 1) elongating the base; 2) increasing the base doping per QW; 3) dense packing of the QWs (decreasing the period a); 4) using contact extensions (increasing b); and 5) optimizing the Fermi-energy $\varepsilon_F^{(c)}$. Base elongation leads to a decrease in the oscillation frequency in the LVR, and it could hardly be compensated at the expense of higher frequency in the HVR. The other ways do not affect the oscillation frequency in the LVR substantially. This means that an oscillation frequency in the HVR of such medium diodes is higher than a maximum frequency for the corresponding short diodes. Exploitation of the HVR oscillatory regime is a reserve to heighten the oscillation frequency for the diodes with the same base length. This becomes important if almost all the HVR is below the optical phonon energy and ballistics conditions are realized.

Snap shots of concentration distributions per one period of oscillation at a voltage in the middle of the LVR are shown in Fig. 7(b). Analogous pictures for the HVR are presented in Fig. 7(c) and (d). The oscillations in the LVR are practically the same as in the short diodes (see Fig. 7(a)). In the HVR, concentration waves localize around a stationary AP, which becomes clearly visible in the middle of the base. The most characteristic detail of the concentration distributions is a space charge wave generated on the left of the AP (in the LDR), then traversing across it and decaying on the right (in the RDR). It does not reach the cathode or reaches it in a destroyed form. Contrary

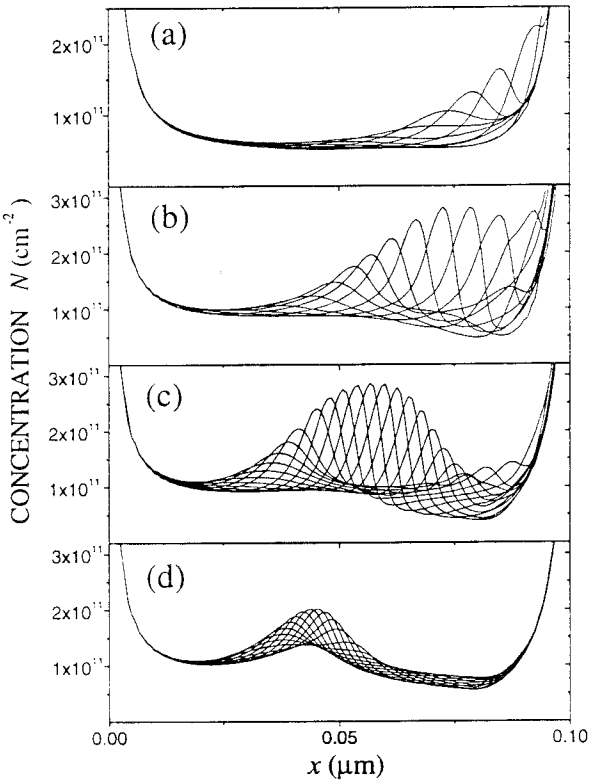

Figure 7. The snapshots of the concentration distributions, $N(x)$, recorded during one period of the oscillation for a short diode (a) - sample (1,1) at 20 mV, and for a medium diode in the LVR (b) and in the HVR (c) and (d) - sample (5/3,1) at 36, 60, and 70 mV, respectively.

to the Gunn domain, the concentration wave is generated and decays in a spatially homogeneous base where there are no artificial beginnings for domain formation but inhomogeneous stationary concentration and potential distributions in the diode base determine the origin and termination points for the wave.

C. Long diodes

Signals of a switch from the medium diode to the long diode are appearance and extension of nonlinear oscillations in the oscillatory portrait and development of diversity of oscillatory regimes. Base elongation induces an increase in U_k as for the medium diodes. A detailed description of the nonlinear oscillatory regimes is out of the scope of this paper. We restrict ourselves to several notes.

1). With an increase in the base length, first of all, nonlinear oscillations appear near U_c and in the neck. Then, the region of nonlinear oscillations around the neck is extended onto the both sides. Regions of quasilinear behavior are forced

out and squeezed, but the region of quasilinear oscillations in the HVR remains ever for very long bases. As a rule, the maximum frequency of oscillations occurs in this part. This frequency is determined by the transit time of holes across a certain short section of the base.

2). Stationary concentration distributions before and after oscillations typically have long enough quasineutral regions. The quasineutral regions, at $U>U_k$, are shortened as the RDR extends.

3). Multidomain solutions with two, three or more APs are characteristic for the long diodes.

4). A picture of oscillations in the long diode depends on the voltage sweep rate: portrait details in the forward and in the reverse directions of CP IVC are different; that is, different oscillatory regimes are induced. This means that oscillatory regimes in the long diodes are multivalued and historically predetermined.

Generally speaking, an elongation of the base leads to lowering frequencies. But among a number of different oscillatory regimes there are high frequency regimes which are inherent to shorter diodes. The strict dependence of the frequency on the base length exists only for short diodes.

VI. Discussion

A. High voltage oscillatory regime

The existence of a long quasineutral NEM-plasma region in the stationary solution is one cause of convective instability of a stationary regime and generation of oscillations. For development of this instability, a length of this region has to exceed some characteristic length:

$$\Lambda = v_c \eta^{-1}, \qquad (5)$$

where $v_c=v(p_c)$ and η is the increment determined by Eq. (1). For $m_N=10^{-28}$ g, $N=N_A/a=(10^{11}\ \mathrm{cm}^{-2})/(3.2\cdot10^{6}\ \mathrm{cm})\approx3\cdot10^{16}\ \mathrm{cm}^{-3}$, $\kappa_d=10.9$ and $v_c=1.2\cdot10^{7}$ cm/s we have $\eta=2.7\cdot10^{12}\ \mathrm{s}^{-1}$ and $\Lambda=44$ nm. A NEM-region of length $\sim\Lambda$ is sufficient to develop instability and to promote an oscillatory regime. Shortening of length Λ and elongation of the NEM-region evoke transition from the short diode to the medium and long diodes. A very short NEM-region is no more homogeneous and quasineutral, it becomes a part of the LDR. Actually, the critical length of the NEM-region for the oscillatory regime depends on damping processes outside the NEM-region and outer loads. For qualitative estimation, we assume that this length is of the order of Λ.

One of the significant results of this work is the discovery of the multivalued behavior of the ballistic diode with NEM-carriers. This behavior consists in the coexistence of the stationary and oscillatory regimes in the same voltage interval. As we have already shown, almost all the HVR or its significant part (see Figs. 3-6) is in such an interval and whether the HVR-oscillations appear or not depends on a turning-on regime.

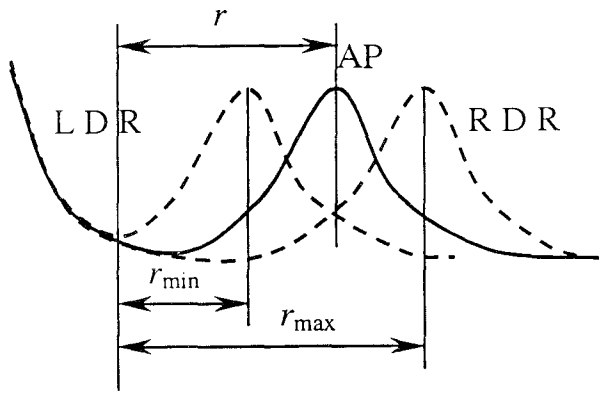

Figure 8. A sketch of the oscillations of the AP and the length of the NEM-region, r, in the HVR. Left boundary of the NEM-region is supposed unchangeable because plasma waves do not deeply penetrate to the left.

The HVR oscillatory regime is due to an oscillatory movement of the nonstationary AP in the middle of the medium diode shown in Fig. 7(d) while the stationary regime is characterized by the stationary AP located actually in the same place. This AP separates two depletion regions, the LDR and RDR. A part of the LDR near the AP is the NEM-region shown qualitatively in Fig. 8. It is of small length and has an inhomogeneous concentration distribution. The stationary regime is stable because interaction of plasma oscillations in the NEM-region with the NEM-carriers that amplifies these oscillations is generally weaker than their interaction with ballistic carriers elsewhere that have a positive mass; this last interaction is a particular case of the Landau damping. In the framework of our approach, this means that the length of the NEM-region, r, is smaller than Λ.

In the HVR-oscillatory regime, the AP oscillates near its stationary position, which leads to alternation of shortening and elongation of the NEM-region to the left of the AP. An effect of the shortening and elongation is asymmetrical because the amplitude of the amplifying plasma waves depends on the length of the NEM-region exponentially. Therefore, if the oscillations of the AP are sufficiently large, gain due to elongation of the NEM-region greatly exceeds damping due to its shortening. Finally, this oscillation regime becomes self-governing for the relatively high oscillation amplitude, and it is referred to as the HVR-oscillation regime. The suggested description has a qualitative character and is used only for illustration of the exact numerical results from Secs. III-V.

The voltages U_c and U_{k0} in Refs. 1, 2 are obtained under two assumptions: 1) an effective anode (source of holes) emits holes with zero energy that means that the tangent line in Fig. 1(a) comes from the origin p=0, ε =0; and 2) there exists a quasineutral NEM plasma region in the diode with zero

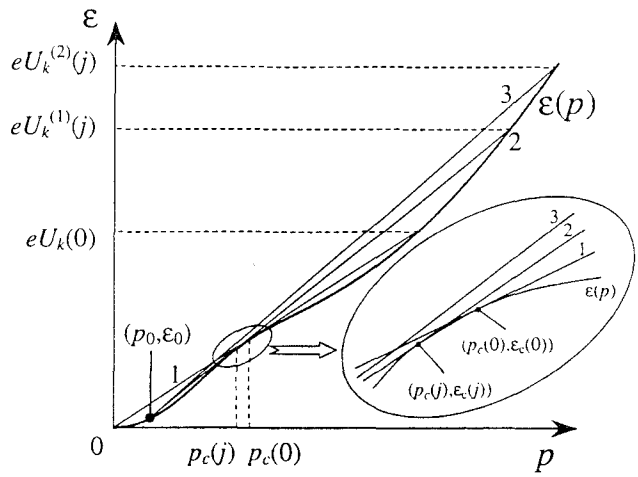

Figure 9. An illustration of variation of voltage U_k as current density increases, $U_k^{(1)}(j)$, and as the NEM-region shortens, $U_k^{(2)}(j)$.

electric field that corresponds to the tangency point (p_c,ε_c) in Fig. 1(a). Actually there is a certain clearance between the Fermi-energy $\varepsilon_F^{(c)}$ and a height of the effective anode eU_M because of finite values of the current density j. Therefore, kinetic energies of the emitted holes are in the interval $(0,\varepsilon_F^{(c)}-eU_M)$. To take into account nonzero energy of the emitted holes, we need to shift an origin point of the tangent line along the dispersion curve to the right and upwards (Fig. 9). Then, the point of intersection $U_k(j)$ is shifted to the right and upwards substantially. This means that $U_k(j)$ is always greater than $U_k(0)$.

In our case, there is one more cause of increasing U_k. If a quasineutral NEM-region in the base is very small, as we see above, we should not require the characteristic straight line from the point $(p_x(0),\varepsilon(0))$ to be tangent at the point (p_c,ε_c) but this line should be directed higher. The deviation of this line from the tangent line is greater as the oscillation amplitude is greater. The extended NEM-plasma region in this regime has dynamic character - it is absent in the stationary solution. These qualitative consideration intends only to illustrate the theoretical results obtained by direct calculations.

Experimental implementation of the HVR is more difficult because of the optical phonon limit $\hbar\omega_o/e$. To use this high-frequency oscillatory regime we have to lower the energy ε_c and, consequently, the whole frequency ranges.

B. Rise in frequency

In the frameworks of GaAs/AlAs material system (selected because of the high quality of p-QWs, especially on the <311>A-GaAs-substrate) and the conditions of ballistic transport, $eU<\hbar\omega_o$ (and $\varepsilon_c<\hbar\omega_o$), the highest generation frequency that we can reach is about 3 THz. To exceed this limit we need to

increase ε_c over $\hbar\omega_o$ and/or to change the material system. An increase in ε_c raises transit velocities as $\sim\varepsilon_c^{1/2}$. But crossing the optical phonon threshold means a substantial shortening of the mean free path and the required base length. Together with the decrease in l we have to increase the packing density of QWs and the doping concentration in order to obtain an oscillatory regime. For example, the increase in ε_c from ~20 meV to ~100 meV requires a decrease in the width w from ~8 nm to ~2-2.5 nm. The period of the structure a should be decreased in the same relation (for example, from 32 nm to 8-10 nm), and the base length should be shortened to 25-30 nm. Further shortening would break the oscillatory regime. These structure reformations raise frequencies up to 8-10 THz. The question whether such a structure is ballistic remains unresolved.

Another way to increase frequency is to replace GaAs with InAs in QWs. The light hole effective mass and mass m_N in the InAs-QWs are smaller than in GaAs. A disadvantage of InAs as the material for p-QWs is the absence of isomorphic wide-gap barrier material. Either InP or AlAs can be used as barrier materials to form pseudomorphic InAs p-QW. Barrier height in these cases is 0.3-0.5 eV [27-29]. These heterostructures can be either a very narrow ($w \leq 2$ nm) in-plane compressed InAs-QW with AlAs-barriers on GaAs-substrate or a multiple QW systems of in-plane compressed InAs-QWs and tensile stressed AlAs- barriers with InGaAs-buffer layers.

VII. Conclusions

We have shown that stationary ballistic hole current through a short p-QW base of the p^+pp^+-diode is unstable because of the NEM-section in the dispersion relation of quantized holes. Quasistationary oscillatory regimes appear in wide voltage intervals with frequencies of oscillations of hole concentration, electric potential and current in terahertz range for bases shorter than 0.3 μm. An oscillatory regime depends on the base length, doping concentration, packing density for multiple QW systems, energy of emitted holes, length of the contact extensions and dispersion relation details.

An oscillatory regime for the so-called short and medium diodes is almost always quasi-monochromatic. Frequencies of oscillations in the voltage intervals below the optical phonon emission reach 2-3 THz for base lengths 0.06-0.1 μm. Oscillatory regimes with substantially nonlinear oscillations appear for the so-called long diodes. These nonlinear oscillations correspond to multidomain concentration waves in the base when several APs traverse the base simultaneously one after another. The oscillatory portrait can be multivalued (at least in some parts) and selection of one regime or another is determined by their previous history.

Adiabatically slow voltage variations allow us to bring to light expended intervals of the overheated and overcooled states. The stationary solutions are metastable in these intervals and oscillatory regimes can be

developed only after a shock voltage excitation. A new oscillatory regime in the HVR (outside the analitically predicted oscillation interval (U_c, U_{k0}); see Fig. 1(a)) has been described in detail. We have shown that this new high frequency regime is conditioned by motion of the nonstationary AP between two depletion regions in the self-organized plasma cavity. The transit distance is much shorter than the entire base length. Therefore, the frequency of oscillations in this regime is higher than in the LVR, and there is a certain reserve to heighten the frequency range without adequate shortening of the base length.

There are no artificially created inhomogeneities in the diode base that could be a nucleus for origin or termination of the concentration waves. Appearance of these waves is a result of spatial-temporal self-organization of electric potential and concentration in the homogeneous base.

Another prospect to heighten the frequency range is based on narrowing the p-QWs and lifting the energy region to $\varepsilon > \hbar\omega_0$. This way could be possible if a mean free path for emission of the optical phonon were 30 nm or longer. Therefore, a study of hole mobility $\mu(T)$ in the temperature range 0-70 K for narrow p-QWs and nonequilibrium hole transport in such wells are very pertinent.

Acknowledgments

The authors thank Serge Luryi for his detailed discussion of our results and Alex Zaslavsky for his repeated suggestions for implementing ballistic diode structures on the basis of p-QWs. We thank William R. McGrath and Boris Karasik for their fruitful talks over possible applications of ballistic generators on the basis of the considered physical effects. The exchange views on some special details with E.M. Gershenzon, G.N. Gol'tsman, and S.K. Tolpygo were also very useful to us. The authors are grateful to D. J. Jenuwine for his reading of the manuscript.

This work has been supported by the NSF (grant ECS 9526112).

Appendix: P-Type GaAs/AlAs Quantum Wells: Short Review

It is well known that holes are poor current conductors compared to electrons: hole mobility in GaAs -bulk samples is 20 times smaller than electron mobility. In InP and InAs, the advantage of electron mobility over hole mobility is even greater. The same situation exists in most direct-gap $A_{III}B_V$-materials. Detailed data of hole mobilities and drift velocities have been presented in review papers Refs. 30, 31.

The small values of hole mobilities are conditioned not only by their small velocity $v=p/m_h$ for a given momentum p (because of a heavy hole mass m_h), but also by their small scattering time τ. In Ref. 32, tunneling–emitted light holes with energy about 0.2 eV have a mean free-path of only 14 nm because of

very strong scattering into a heavy hole band. Electrons under analogous conditions run 5-7 times further without scattering.

For quantized holes, however, the situation could be different since the longitudinal effective mass in the bottom of the HH1-subband is much smaller. This means that their velocity is higher than the heavy hole velocity and the density of states where they could be scattered to is noticeably smaller than it is in the bulk case. According to the data for the infinitely deep square p-GaAs QW [16-19], the effective mass m_{HH1} at $p \to 0$ is in the range of $(0.1\text{-}0.12)m_0$ for different well orientations while the heavy hole mass is $0.51m_0$, where m_0 is the free electron mass. Therefore, we should expect a relatively high mobility of the HH1-holes if a Fermi–level position is in a section with small mass m_{HH1}, hole concentration N is near 10^{11} cm^{-2} and temperature is outside the temperature interval with predominating roughness scattering.

In practice, an increase in mobility has not been observed yet: hole mobility in a narrow modulation-doped square QW is always smaller than mobility in a quasitriangle MDH QW. In the MDH QW, the HH1 subband is split into two subbands HH1$^{(\pm)}$. As a result, most holes are in the heavier of the two [20,33,34]. Though most holes are heavy, these MDH QWs provide the highest hole mobility in a wide temperature range. The best GaAs/$Al_xGa_{1-x}As$ MDH QWs grown on <100>GaAs-substrates have hole mobility higher than 10^5 cm^2/Vs at T=4.2 K ($1.2\cdot10^5$ cm^2/Vs in Ref. 35, $1.4\cdot10^5$ cm^2/Vs in Ref. 36). The hole mobility at T<60 K is determined mainly by acoustic phonon and heterojunction roughness scattering if spacer and buffer layers are sufficiently wide and pure.

Figure 10 demonstrates three experimental dependencies $\mu(T)$ adopted from Ref. 37. They are obtained for the MDH QWs with x=0.5 and hole concentrations $(1.8\text{–}2.5)\cdot10^{11}$ cm^{-2}. One of these samples has the record mobility for <100>-orientation: $\mu=2.3\cdot10^5$ cm^2/Vs. We can conclude that phonon scattering dominates for higher temperatures where all three curves coincide while the contribution of the roughness scattering becomes noticeable at lower temperatures where mobilities are different. In QWs grown on <311>A-GaAs-substrates, roughness scattering is displayed much more weakly due to the special ordering of these roughnesses [38]. Therefore, the low-temperature hole mobility can be much higher and it increases with decreasing temperature down to very low temperatures. Two $\mu(T)$-dependencies adopted from Refs. 39 and 40 for MDH QWs grown on <311>A-GaAs-substrates with current directed along [233]-axis are shown in Fig. 10. All the curves are in conformance with each other.

Figure 10 demonstrates that the possible values of μ are restricted by $4\cdot10^5$cm^2/Vs at 4.2 K and can exceed 10^6 cm^2/Vs at 2 K (both the former and the latter are now obtained experimentally - see Refs. 36, 40, 41). Even higher values of μ are obtained in modulation doped square GaAs-QWs with two heterojunctions of considerable width [42-44] (w=15 nm). This mobility

substantially decreases with the narrowing of the QW. For example, $0.75 \cdot 10^5$ cm^2/Vs and $0.65 \cdot 10^5$ cm^2/Vs are measured for square QWs of 7 and 8.5 nm width grown on <311>A-GaAs-substrate with hole concentrations $0.33 \cdot 10^{11}$ and $0.45 \cdot 10^{11}$ cm^{-2}, respectively [45]. This decrease in mobility is due to increased roughness scattering. We assume that hole mobilities in these QWs are equalized with the best MDH QWs at 20-30 K and then exceed them at higher temperatures (see the dashed curve in Fig. 10 for expected dependency $\mu(T)$ in a narrow p-QW).

These conclusions are confirmed by measured small hole masses in narrow square p-QWs. In Ref. 46, the hole mass of $0.1m_0$ for GaAs/AlGaAs-QW of 2.2 nm width and $(0.14\text{-}0.17)m_0$ for 5.5 nm, 7.7 nm, and 11.2 nm QW's widths are measured from magnetoreflectivity data. The HH1-hole masses $(0.15\text{-}0.17)m_0$ for w=7 and 8.5 nm are obtained from cyclotron resonance data [45] for weak and intermediate magnetic fields. Reference 47 demonstrates the agreement of experimental data on luminescence in multiple p-type 3.3-9.8 nm GaAs/$Al_xGa_{1-x}As$-QWs with theoretical predictions including both the small HH1-effective masses and the NEM-sections. Finally, we mention two Refs. 48 and 49 on resonance magnetotunnelling across narrow (6.8, 4.2, and 2.5 nm) GaAs/AlAs-QWs. The NEM-sections in the obtained dependencies of resonance voltage on magnetic field are clearly displayed.

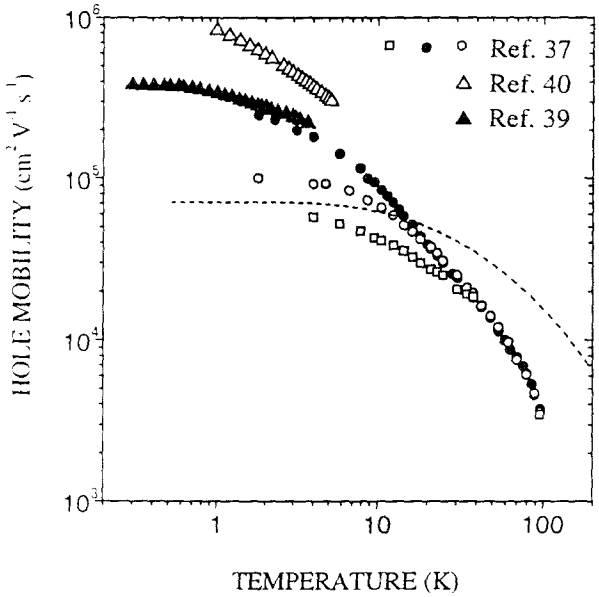

Figure 10. Hole mobility, μ, as a function of temperature, T, in GaAs/AlGaAs QWs. Data shown by □, ○, and ● are taken from Ref. 37, ▲ – from Ref. 39, and △ – from Ref. 40. The dashed line shows an expected behavior for $\mu(T)$-relation for a narrow p-QW.

We assume that a square p-QW with hole mobility $\mu=0.5\cdot10^5$ cm^2/Vs and hole effective mass $m=0.15m_0$ at a Fermi -surface is suitable for the ballistic diode bases. Related scattering time $\tau=m\mu/e=4.3\cdot10^{-12}$ s and mean velocity $v=1.1\cdot10^7$ cm/s result in mean free path of $L\approx0.5$ μm. Below, we consider base lengths $l=0.1$ μm and rarely $l=0.2$ μm with oscillation frequencies, $f=\omega/2\pi$, that exceed 1 THz and 0.7 THz respectively. Therefore, the required ballistic transport conditions ($l<<L$; $\omega\tau>>1$) are met if τ depends on hole energy weakly in the interval 0 to $\hbar\omega_0$ (in GaAs it is equal to 37 eV). Note, roughness scattering and acoustic phonon scattering depend weakly on energy [50].

References:

[1]Z.S. Gribnikov, A.N. Korshak, Semiconductors **28**, 812 (1994).
[2]Z.S. Gribnikov, A.N. Korshak, in *Quantum Confinement.Physics and Applications*, edited by M. Cahay, S. Bandyopadhyay, J-P. Leburton, A.W. Kleinsasser, M.A. Osman (Electrochem. Soc., Pennington, NJ, 1994), p.34.
[3]N.Z. Vagidov, Z.S. Gribnikov, A.N. Korshak, Semiconductors **29**, 1014 (1995).
[4]N.Z. Vagidov, Z.S. Gribnikov, A.N. Korshak, JETP Lett. **61**, 38 (1995).
[5]Z.S. Gribnikov, A.N. Korshak, N.Z. Vagidov, Lithuanian J. Phys. **35**, 495 (1995).
[6]Z.S. Gribnikov, A.N. Korshak, N.Z. Vagidov, J. Appl. Phys. **80**, 5799 (1996).
[7]R.Q. Yang, J.M. Xu, Appl. Phys. Lett. **59**, 315 (1991).
[8]N.Z. Vagidov, Z.S. Gribnikov, A.N. Korshak, in *Hot Carriers in Semiconductors*, edited by K. Hess, J-P. Leburton, U. Ravaioly (Plenum, New York, 1995), p.183.
[9]I.L. Aleiner, E.L. Ivchenko, Semiconductors **27**, 330 (1993).
[10]G. Bir, E. Pikus, *Symmetry and Strain Induced Effects in Semiconductors* (Wiley, New York, 1974).
[11]A.N. Korshak, Z.S. Gribnikov, N.Z. Vagidov, in *Hot Carriers in Semiconductors*, edited by K. Hess, J-P. Leburton, U. Ravaioly (Plenum, New York, 1995), p.187.
[12]N.Z. Vagidov, Z.S. Gribnikov, A.N. Korshak, Semiconductors **31**, 150 (1997).
[13]M.L. Cohen, J.R. Chelikowsky, *Electronic Structure and Optical Properties of Semiconductors* (Springer-Verlag, Berlin, 1988).
[14]B.K. Ridley, *Quantum Processes in Semiconductors* (Clarendon Press, Oxford, 1993).
[15]Yu.M. Sirenko, J.B. Leon, B.C. Lee, K.W. Kim, M.A. Littlejohn, M.A. Stroscio, G.J. Iafrate, Phys. Rev. B **55**, 4360 (1997).
[16]S.S. Nedorezov, Sov. Phys. Solid State **12**, 1814 (1971).
[17]M.I. D'yakonov, A.V. Khaetskii, Sov. Phys. JETP **55**, 917 (1982).
[18]A.V. Chaplik, L.D. Shvartsman, Sov. Phys. Surf. Phys. Chem. Mech. **2**, 73 (1982).
[19]G. Shechter, L.D. Shvartsman, J.E. Golub, Phys. Rev. B **51**, 10857 (1995).
[20]D.A. Broido, L.J. Sham, Phys. Rev. B **31**, 888 (1985).
[21]Z.S. Gribnikov, A.N. Korshak, N.Z. Vagidov, Z.M. Alexeeva, in *Proceedings of the 23 International Conference on Physics of Semiconductors*, edited by M. Schefler, R. Zimmerman (World Scientific, Singapore, 1996), **4**, p.3287.
[22]A.N. Korshak, Z.S. Gribnikov, N.Z. Vagidov, S.I. Kozlovsky, V.V. Mitin, Phys. Stat. Sol. (b), **204**, 80 (1997).
[23]A.N. Korshak, Z.S. Gribnikov, N.Z. Vagidov, S.I. Kozlovsky, V.V. Mitin, Micro-electronic Engineering **43-44**, 429 (1998).

[24]V.V. Mitin, Z.S. Gribnikov, A.N. Korshak, in *Physics of Semiconductor Devices*, edited by V. Kumar, S.K. Agarwal (Narosa Publ.House, New Delhi, 1998) **1**, p.131.
[25]R. Winkler, U. Rössler, Phys. Rev. B **48**, 8918 (1993); Surf. Sci. **305**, 295 (1994).
[26]L.A. Andreani, A. Pasquarello, F. Bassani, Phys. Rev. B **36**, 5887 (1987).
[27]J.R. Waldrop, R.W. Grant, E.A. Kraut, Appl. Phys. Lett. **54**, 1878 (1989).
[28]S. Tiwari, D.J. Frank, Appl. Phys. Lett. **60**, 630 (1992).
[29]S.-H. Wei, A. Zinger, Appl. Phys. Lett. **72**, 2011 (1998).
[30]R.A. Kiehl, in *High Frequency Heterostructure Devices*, edited by R.A. Kiehl, T.C.L.G. Sollner (*Semiconductors and Semimetals*, **41**, Academic Press, Boston, 1994), p.219.
[31]E.P. O'Reilly, Semicond. Sci. Techn. **4**,121 (1989).
[32]M. Heiblum, K. Seo, H.P. Meier, T.W. Hickmott, Phys. Rev. Lett. **60**, 828 (1989).
[33]U. Ekenberg, M. Altarelli, Phys. Rev. B **32**, 3712 (1985).
[34]E. Bangert, G. Landwehr, Surf. Sci. **170**, 593 (1986).
[35]B.E. Cole, S.O. Hill, Y. Imanaka, Y. Shimamoto, W. Batty, J. Singleton, J.M. Chamberlain, N. Miura, M. Henini, T. Cheng, Surf. Sci. **361/362**, 464 (1996).
[36]B.E. Cole, F.M. Peeters, A. Ardavan, S.O. Hill, J. Singleton, W. Batty, J.M. Chamberlain, A. Polisski, M. Henini, T.Cheng, J. Phys: Condens. Matter **9**, 3163 (1997).
[37]E.E. Mendez, W.I. Wang, Appl. Phys. Lett. **46**, 1159 (1985).
[38]W. Langbein, D. Lüerssen, H. Kalt, J.V. Hvam, W. Braun, K. Ploog, Phys. Rev. B **54**, 10784 (1996).
[39]W.I. Wang, E.E. Mendez, Y. Iye, B. Lee, M.H. Kim, G.E. Stillman, J. Appl. Phys. **60**, 1834 (1986).
[40]M. Henini, P.J. Rodgers, P.A. Crump, B.L. Gallagher, Appl. Phys. Lett. **65**, 2054 (1994).
[41]P.J. Rodgers, B.L. Gallagher, M. Henini, G. Hill, J. Phys: Condens..Matter **5**, L565 (1993).
[42]J.J. Heremans, M.B. Santos, M. Shayegan, Appl. Phys. Lett. **61**, 1652 (1992); Surf. Sci. **305**, 348 (1994).
[43]I.S. Millard, N.K. Patel, M.Y. Simmons, E.H. Linfield, D.A. Ritchie, G.A.C. Jones, M. Pepper, Appl. Phys. Lett. **68**, 3323 (1996).
[44]A.R. Hamilton, M.Y. Simmons, F.M. Bolton, N.K. Patel, I.S. Millard, J.T. Nicholls, D.A. Ritchie, M. Pepper, Phys. Rev. B **54**, R5259 (1996).
[45]B.E. Cole, J.M. Chamberlain, M. Henini, T. Cheng, W. Batty, A. Wittlin, J.A.A. Perenboom, A. Ardavan, A. Polisski, J. Singleton, Phys. Rev. B **55**, 2503 (1997).
[46]A.S. Plaut, J. Singleton, R.J. Nicholas, R.T. Harley, S.R. Andrews, C.T.B. Foxon, Phys. Rev. B **38**, 1323 (1988).
[47]J.A. Kash, M. Zachau, M.A. Tishler, U. Ekenberg, Surf. Sci. **305**, 251 (1994).
[48]R.K. Hayden, D.K. Maude, L. Eaves, E.C. Valadares, M. Henini, F.W. Sheard, O.H. Huges, J.C. Portal, L. Cury, Phys. Rev. Lett. **66**, 1749 (1991).
[49]R.K. Hayden, L. Eaves, M. Henini, E.C. Valadares, O. Kühn, D.K. Maude, J.C. Portal, T. Takamasu, N. Miura, U. Ekenberg, Semicond. Sci. Techn. **9**, 298 (1994).
[50]W. Walukievich, Phys. Rev. B **31**, 5557 (1985); Phys. Rev. B **37**, 8530 (1988).